PAPER

Several different charge transfer and Ce^{3+} localization scenarios for Rh–CeO$_2$(111)

Zhansheng Lu,[a] Zongxian Yang,[a] Kersti Hermansson*[bc]
and Christopher W. M. Castleton*[d]

We present DFT+U based electronic structure calculations in a $p(3 \times 3)$ slab supercell, for low coverages of atomically dispersed Rh interacting with the CeO$_2$(111) surface, comparing Rh as an adatom, and as a dopant substituted into the surface layer. We find that, energetically, a Rh atom approaching a ceria(111) surface with both sparse O and Ce vacancies present strongly prefers to heal the Ce vacancies, but next it prefers to adsorb on a stoichiometric region rather than healing an O vacancy. In the adatom system, Rh is oxidized by electron transfer to a 4f orbital on one Ce ion in the surface layer, which is then nominally converted from Ce$^{4+} \rightarrow$ Ce^{3+} (*i.e.* Rh adatoms are single donors). We show that there are a number of different local minima, with Ce^{3+} localization at 1st, 2nd or 3rd nearest neighbour Ce sites. The second neighbour is the most stable, but all are close in energy. In the Rh-doped system (Rh replaces Ce), Rh is oxidized by charge transfer to neighbouring O atoms, and Rh doping leads to deep acceptor and donor states. Rh is not stable in the O sublattice. Moreover, based on vacancy formation energies, we find that oxygen vacancy formation is strongly enhanced in the vicinity of Rh dopants, but slightly suppressed in the vicinity of Rh adatoms.

1. Introduction

Among the multiple roles of CeO$_2$ in catalysis, one of the most important is to store and release oxygen, a process which is promoted by noble metals such as Pd, Pt, and Rh.[1,2] Here, we focus on atomically dispersed Rh at low coverage on ceria (111), the most stable low index surface.[3–5] In principle, Rh atoms can form adatom species, heal vacancies, or "dope" the surface by replacing individual cations or anions. Here we present a density functional theory (DFT)[6] study comparing the energetics of these different possibilities, and the resulting geometric and electronic structures. We will use a $p(3 \times 3)$ surface supercell which enables us to compare alternative Ce^{3+} localization patterns, their accompanying structures, stabilities and charge transfer character.

Rh–ceria systems have been studied intensively by experiments (see ref. 7 and references therein for earlier work), but a clear picture of the location and structure of low coverage Rh on ceria(111) has not emerged. The cerium ions in pure stoichiometric ceria are nominally in the Ce^{4+} state, with no 4f

electrons, but it has long been known that the formation of oxygen vacancies leads to the appearance of Ce^{3+} ions.[8,9] Pfau *et al.*[10] showed that *Ce^{3+} ions also appear after Rh adsorption*. They deposited Rh from less than 0.1 monolayers (ML) up to 2.2 ML on ceria thin films, and found several regimes: for coverages below about 0.3 ML, they found that *isolated Rh adatoms dominate*; above 0.3 ML they found evidence of Rh aggregation, leading to the formation of *metallic Rh layers* from 2 ML. For *all* coverages, Ce3s XPS spectra showed the appearance of Ce^{3+} ions near the surface following Rh deposition. At low coverages (the focus of our paper), Pfau *et al.* attributed this to the formation of neutral Rh adatoms, which they suggested catalysed O desorption, which in turn led to Ce^{3+} creation. They acknowledged that charge transfer from Rh to Ce in the ground state was an alternative interpretation, but considered it unlikely due to the similarity of the work functions of *bulk* Rh and CeO$_2$. However, they did find a new HREELS peak upon Rh adsorption, which they interpreted as (excited state) charge transfer from Rh4d to Ce4f, and suggested that this implies that Ce and Rh are close together, and hence that Rh must occupy a Ce-top adsorption site. Hosokawa *et al.*,[11] on the other hand, used XANES to show that rather than remaining neutral, *Rh is oxidized* by the ceria surface, though not as much as in, say, Rh$_2$O$_3$. They also used XAFS measurements to show that Rh is "highly dispersed" on the surface, and forms Rh–O–Ce structures, indicating adsorption either above or neighbouring O, rather than on Ce as suggested by Pfau *et al.* Wang *et al.*[12] also suggested that the Rh becomes charged, using XPS to identify both the Rh^0/Rh$^{\delta+}$ and

[a] College of Physics and Electronic Engineering, Henan Normal University, Xinxiang, 453007, China

[b] Materials Chemistry, The Ångström Laboratory, Uppsala University, Box 538, SE-75121 Uppsala, Sweden. E-mail: kersti@mkem.uu.se

[c] Department of Theoretical Chemistry, Royal Institute of Technology, Roslagstullsbacken 15, SE-106 91 Stockholm, Sweden

[d] School of Science and Technology, Nottingham Trent University, Nottingham, NG11 8NS, UK. E-mail: christopher.castleton@ntu.ac.uk

This journal is © The Royal Society of Chemistry 2014

J. Mater. Chem. A, 2014, **2**, 2333–2345 | **2333**

the Ce^{4+}/Ce^{3+} redox couples, and temperature programmed reduction (TPR) to associate the redox couples with the higher catalytic activity of $Rh–CeO_2/Al_2O_3$.

Further structural information comes from the work of Gayen et al.,[13] who prepared Rh/ceria model catalysts containing 0.5–2 atom% Rh, which they characterised using a range of X-ray and chemical techniques. They again showed that Rh adsorption involves the creation of Ce^{3+} ions, and that Rh is dispersed over the ceria surface, with no indication of the presence of Rh metal, or of the oxides Rh_2O_3, RhO_2 and $CeRhO_3$, or of RhO-like species. They interpreted their H_2 uptake data as indicating the presence of *three different Rh sites* on the surface. They also reported Rh–O and Rh–Ce distances of ∼2.0 Å and 3.2 Å, respectively, together with rough coordination numbers by fitting to EXAFS data. The data indicated that Rh is mostly associated with oxygen, and they interpreted this and their other data as indicating that Rh atoms can *actually replace Ce atoms*, principally in the surface layers, to form $Ce_{1−x}Rh_xO_{2−δ}$, leading to a higher catalytic activity for CO oxidation. It has been suggested[14] that such substitution is a general method for modifying the reactivity of oxide-based catalysts.

To summarize the experimental data: many different forms of Rh have been found or suggested for Rh in contact with ceria, with isolated Rh atoms at low coverages (below ∼0.3 ML), and agglomeration and eventually metallic Rh at higher coverages. *In this paper* we will present a systematic study to highlight the preferred state and behaviour of an isolated Rh atom on and in a $CeO_2(111)$ surface.

To our knowledge only three DFT studies have considered Rh doping of CeO_2. The first[15] did not contain any surfaces. The second[16] described the effect of various transition metal dopants (including Rh) on dissociative methane adsorption and oxygen vacancy formation, using a $p(2 × 2)$ supercell, hence 25% surface layer doping. However, it did not give details of the Rh–ceria system itself, except that the Rh is octahedrally coordinated with nearest neighbour distances of 2.16–2.49 Å. The third[17] considered fifteen different transition metals doped into the *second* subsurface Ce layer in slab geometry models of the (111) and (110) surfaces. In comparison with experiment they showed that the oxygen vacancy formation energy gives a reasonable measure of the catalytic activity of doped ceria, and also that all fifteen of their dopants lowered the formation energy (increased the activity) relative to pure ceria – in the case of Rh by around 0.9 eV.

As far as computational Rh *adatom*–ceria (111) studies are concerned, a few[18–24] have focused on chemical processes and/or Rh cluster formation but without presenting details for low coverage Rh/ceria structures, which are the focus of the present study (see also the recent review of defects on ceria[25]). Two have reported low coverage Rh adatom structures on ceria(111),[21,26] showing that the most stable adatom site is in a three-fold hollow between three surface O ions. Although detailed electronic structure and analysis was not given, it was reported that adsorption involves charge transfer from the Rh to the surface, and that this transferred charge enters the Ce4f states of a single cerium ion, nominally changing it from Ce^{4+} to Ce^{3+}. When

similar calculations were instead performed in a larger $p(3 × 3)$ surface supercell[26] it was possible to show that these Ce^{3+} ions are located at the next nearest neighbour (NNN) location relative to the adsorbed Rh. However, we will show that several alternative Ce^{3+} locations exist, and these have not been reported or discussed earlier in the literature. This is an issue of considerable current interest, as it has recently been shown[27–30] that Ce^{3+} ions formed together with oxygen vacancies exhibit a wide variety of competing low lying states, involving the *nearest neighbour* (NN), *next nearest neighbour* (NNN) and *next next nearest neighbour* (NNNN) and further shells of Ce ions around the vacancy, and that the resulting localization patterns are closely coupled to the structure and properties of the vacancies. In the present paper we will explore this issue in some detail, as well as the detailed electronic structure of the ground state.

In summary: some experimental studies suggest Rh doping, some suggest the presence of neutral Rh adatoms above Ce sites, and others suggest Rh adatoms above O, with charge transfer from Rh to ceria. Previous DFT results for Rh adatoms indicate an O-hollow site, with charge transfer, but other locations, such as surface doping and/or vacancy healing, have not been considered.

In our paper we provide answers to the following questions:

(i) If a Rh atom approaches an arbitrary ceria(111) surface containing both perfect regions and regions with O or Ce vacancies, where does it want to go and what does it want to do?

(ii) Which of the two – Rh adsorption or Rh doping – has the largest effect on the O vacancy formation energy (and thus also the oxygen storage capacity)?

(iii) If Rh adsorbs over surface O atoms, how much charge transfer is there from Rh and where do(es) the electron(s) go? Is there maybe a multitude of possible low energy Ce^{3+} localization sites, like that found for the electrons released *via* O vacancy formation?

(iv) And, on a more practical note: we use a $p(3 × 3)$ cell in our calculations, but many calculations in the literature use (2 × 2) cells for metal/oxide interfaces. Are the consequences important?

2. Computational details

2.1 Calculation details and models used

We consider three modified $CeO_2(111)$ surface systems: (a) Rh_x/CeO_2 (Rh adatom), (b) $Ce_{1−x}Rh_xO_2$ with $x = 0.111$ in the surface layer (Rh doped onto the Ce sublattice), and (c) $CeRh_xO_{2−x}$ with $x = 0.111$ in the surface layer (Rh doped onto the O sublattice), and will also report the formation energies of single surface oxygen vacancies in the presence of Rh.

DFT calculations were carried out under periodic boundary conditions (PBCs), using the plane-wave based VASP code,[31,32] with the PAW method.[33] The Ce5s5p5d4f6s, O2s2p, and Rh4d5s electrons were treated as valence electrons and plane waves were included up to 30 Ry (408 eV). We treat the strong correlation effects amongst Ce4f electrons using the Dudarev form of the GGA+U functional[34] together with the Perdew–Burke–Ernzerhof (PBE) form of GGA.[35] We used $U = 5$ eV, based on the analysis made in ref. 4, 5 and 36–40.

2334 | *J. Mater. Chem. A*, 2014, **2**, 2333–2345

This journal is © The Royal Society of Chemistry 2014

CeO_2 is a wide band gap semiconductor, with the cubic $Fm\bar{3}m$ structure of CaF_2 and an experimental room temperature lattice parameter of $a = 5.41$ Å, or $a_0 = 5.39$ Å when extrapolated to 0 K.[40,41] Our PBE+U equilibrium lattice parameter is 5.48 Å.

The (111) surface was modelled using a slab geometry comprising 4 (O–Ce–O) triple layers (altogether 108 atoms) and a 15 Å vacuum gap, see Fig. 1a. We will refer to the three atomic layers in the surface triple layer as T1a (O), T1b (Ce) and T1c (O), and those in the second triple layer as T2a (O), T2b (Ce) and T2c (O). The surface supercell chosen was a $p(3 \times 3)$ supercell, hence contained $Ce_{36}O_{72}$ for the clean slab. Some comparative results are given for $p(2 \times 2)$. The in-plane dimensions were fixed at the calculated equilibrium bulk lattice parameter (5.48 Å). In addition, the positions of ions in the bottom six atomic layers (dashed rectangular box in Fig. 1a) were fixed at their optimized bulk atomic positions to mimic the bulk. In all cases the remaining 6 atomic layers (and the Rh atom) were allowed to relax until the force on each atom was less than 0.02 eV Å^{-1}. For *Rh adsorption*, one Rh atom was placed at different positions above one face of the slab while for *Rh doping* it was modelled by replacing either one oxygen (in layer T1a) or cerium (in layer T1b) atom by Rh, giving a doping concentration around 3% for the slab, or 11% for the surface triple layer.

Brillouin-zone integrations were performed using Monkhorst-Pack (MP) grids[42] of $(2 \times 2 \times 1)$ for the $p(3 \times 3)$ supercell and $(4 \times 4 \times 1)$ for the $p(2 \times 2)$ supercell, together with a Gaussian smearing[43] of 0.2 eV. Some checks on convergence will be presented in Section 2.3.

2.2 Energies calculated

For the adatom system, we evaluate the adsorption energy:

$$E_{\text{ads}} = E(\text{Rh}/\text{CeO}_2) - [E(\text{CeO}_2) + E_{\text{ref}}(\text{Rh})] \quad (1)$$

where $E(\text{Rh}/\text{CeO}_2)$ and $E(\text{CeO}_2)$ are the total energies of the same supercell with and without the Rh adatom, and $E_{\text{ref}}(\text{Rh})$ is the reference energy for the source of Rh atoms. The more negative the value of E_{ads}, the stronger the adsorption. We consider two possible reference states for $E_{\text{ref}}(\text{Rh})$: (i) the energy of a free Rh (vapour) atom, $E(\text{Rh}_{\text{gas}})$, and (ii) the energy per atom of Rh in its standard state at room temperature, *i.e.* Rh metal, $E(\text{Rh}_{\text{solid}})$, (calculation details below). These correspond to the Rh–CeO_2 system in equilibrium with the two possible experimental extremes. Most other experimental conditions should produce values somewhere in between.

For Rh incorporated into the Ce sublattice, we calculate the substitution energy as

$$E_{\text{doping}} \text{ at Ce site} = [E(\text{Rh}_x\text{Ce}_{1-x}\text{O}_2) + E_{\text{ref}}(\text{Ce})] \\ - [E(\text{CeO}_2) + E_{\text{ref}}(\text{Rh})] \quad (2a)$$

where $E_{\text{ref}}(\text{Ce})$ is the cerium reference energy. Again, the more negative E_{doping} the more stable the Rh–ceria system. Here we also use two limiting reference states for $E(\text{Ce})$: (i) the free Ce (vapour) atom, $E(\text{Ce}_{\text{gas}})$, and (ii) the energy per atom of Ce metal, $E(\text{Ce}_{\text{solid}})$. This distinction between experimental conditions, and hence reference energies, is particularly important here since we wish to compare the adsorbed Rh with the incorporated/doped Rh. The value of E_{doping} at equilibrium will vary greatly with conditions (temperature, pressure and chemical composition of the gas environment *etc.*) and a full study of all possible sets of conditions and sample histories lies beyond the scope of this paper. However, a rough idea of the spread of possible values can be obtained by considering the four possible (extreme) combinations of $E_{\text{ref}}(\text{Rh})$ and $E_{\text{ref}}(\text{Ce})$.

For Rh incorporated into the O sublattice, we calculate the substitution energy as

$$E_{\text{doping}} \text{ at O site} = [E(\text{Rh}_x\text{CeO}_{2-x}) + E_{\text{ref}}(\text{O})] \\ - [E(\text{CeO}_2) + E_{\text{ref}}(\text{Rh})] \quad (2b)$$

where $E_{\text{ref}}(\text{O})$ is the oxygen reference energy, here taken as $\frac{1}{2}E(\text{O}_2)$, *i.e.* half the total energy of an *oxygen dimer*. Our PBE value for $E(\text{O}_2)$ is -9.39417 eV.
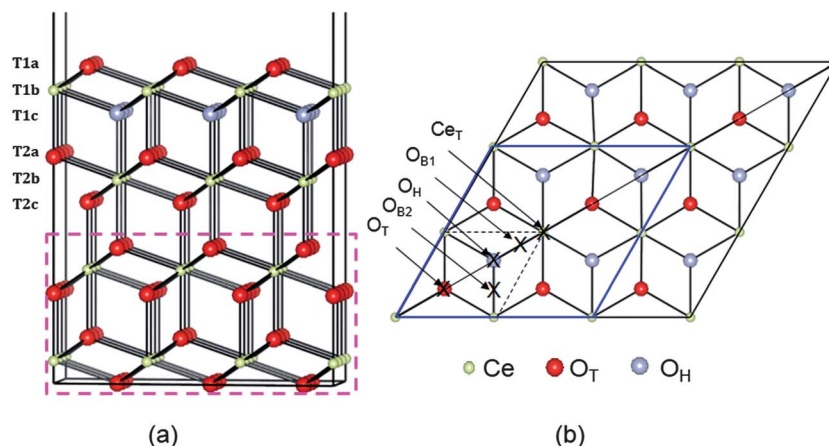

Fig. 1 (a) Side view of the four O–Ce–O triple-layer $p(3 \times 3)$ slab model supercell used for the CeO_2(111) surface. The bottom two triple layers (dashed rectangular box) are fixed at optimized bulk positions. (b) Top view of the supercell, with the labels for the five high symmetry adsorption sites marked to the left of the figure (B stands for bridge, H for hollow and T for top).

In many cases, substitutional doping can formally be seen as two distinct processes: forming a vacancy and healing it using Rh. The first is connected with the vacancy formation energies

$$E_{vac} \text{ at the Ce site} = [E(Ce_{1-x}O_2) + E_{ref}(Ce)] - [E(CeO_2)] \quad (3a)$$

and

$$E_{vac} \text{ at the O site} = [E(CeO_{2-x}) + E_{ref}(O)] - [E(CeO_2)] \quad (3b)$$

The second stage, healing the vacancy, is interesting in its own right, since surfaces sometimes contain a significant concentration of vacancies. The healing energy can be defined as

$$E_{healing} \text{ at the Ce vacancy site} = [E(Rh_xCe_{1-x}O_2)] - [E(Ce_{1-x}O_2) + E_{ref}(Rh)] \quad (4a)$$

and

$$E_{healing} \text{ at the O vacancy site} = [E(Rh_xCeO_{2-x})] - [E(CeO_{2-x}) + E_{ref}(Rh)] \quad (4b)$$

Calculation of reference energies. $E_{ref}(Rh)$ was calculated for *bulk fcc Rh metal* using the primitive unit cell, and an $(8 \times 8 \times 8)$ MP k-point grid, obtaining an optimized lattice constant for the fcc crystallographic cell of 3.842 Å. $E_{ref}(Ce)$ was calculated for *bulk fcc Ce metal* using the primitive unit cell and a $(4 \times 4 \times 4)$ MP k-point grid, obtaining an optimized lattice constant of 5.35 Å. *The free atoms*, $E_{ref}(Rh)$ and $E_{ref}(Ce)$, and the oxygen *dimer*, $E_{ref}(O)$, were calculated using a $10 \times 11 \times 12$ Å unit cell, together with Γ point only k-point integration, full spin polarization and full O–O distance optimization. The optimized O–O distance obtained was 1.29 Å.

2.3 Convergence checks

In order to assess the accuracy of our results, we have performed some additional calculations at the relaxed structure of our most stable Rh adatom configuration (see Section 3.2 for the structure), but with increased basis set, k-point integration, *etc.* (additional relaxation was not performed). We find that the adsorption energy E_{ads} changes by only 0.003 eV if we increase the k-point integration grid to $4 \times 4 \times 1$. If we increase the plane wave cutoff to 700 eV the adsorption energy increases by 0.02 eV, but if we add an additional 5th triple layer on the bottom of the slab (*i.e.* 15 atomic layers) then it decreases by 0.02 eV (note that Krcha *et al.*[16] found a need for 5 or more triple layers for some adatoms, *e.g.*, Ag, V, W, but not for Rh). Finally, adding dipole corrections perpendicular to the surface alters the energies by 0.001 eV. Overall, our main results are therefore expected to be accurate to around 0.01 eV, apart from errors arising from the choice of DFT functional itself.

3. Results

3.1 The fate of a Rh atom arriving at the ceria(111) surface

If a Rh atom approaches an arbitrary ceria(111) surface, one of five things might be expected:

1. It can adhere as an adatom (and then possibly diffuse into the material as an interstitial).
2. It can "heal" a cerium vacancy.
3. It can "heal" an oxygen vacancy.
4. It can kick out and replace an existing cerium ion.
5. It can kick out and replace an existing oxygen ion.

Options 2 and 4, and options 3 and 5 lead to the same endpoints, namely Rh doped substitutionally into the cerium or oxygen sublattices, respectively (assuming subsequent desorption where applicable). Table 1 shows the limiting energies for each process: any value in between is possible, depending on the experimental conditions (the partial pressures of oxygen, Rh and Ce, the physical state of reactants *etc.*). Clearly, any cerium vacancies present will be filled first (line 2 in Table 1), leading to Rh doping of the Ce sublattice; details in Section 3.3 below. After that, Rh is most likely to attach as an adatom (line 1 in Table 1), as discussed in Section 3.2. Replacement of a cerium ion (line 4) is energetically disfavoured. Replacement of an oxygen ion (line 5) or filling an oxygen vacancy (line 3) turns out to be unstable. In all attempts to examine this structure the Rh instead relaxes back out of the oxygen site, to leave a Rh adatom next to an oxygen vacancy. This resulting structure will be discussed in Section 3.4, together with vacancy formation next to Rh adatoms and Rh dopants in the Ce sublattice.

Table 1 Energy data for the Rh–ceria(111) systems studied in this paper, given with respect to different reference states for Rh and Ce

	E_{ads}, $E_{healing}$ or E_{doping} (eV) w.r.t.[a]			
	Rh gas		Rh solid	
	Ce solid	Ce gas	Ce solid	Ce gas
Rh adatom at O_H on $CeO_2(111)^b$	−3.37	−3.37	+2.53	+2.53
Rh-healing a Ce vacancy in layer T1b	−10.22	−10.22	−4.32	−4.32
Rh-healing an O vacancy in layer T1a	Unstable[e]	Unstable[e]	Unstable[e]	Unstable[e]
Rh-doping@Ce site[c]	+5.44	+8.45	+11.34	+14.35
Rh-doping@O site[d]	Unstable[e]	Unstable[e]	Unstable[e]	Unstable[e]

[a] Energies given with respect to (w.r.t.) all four extreme combinations of Rh and Ce reference energies. [b] With NNN localization of Ce4f electrons, since this is the most favourable. [c] Equivalent to Ce vacancy formation + Rh healing. [d] Equivalent to O vacancy formation + Rh healing. [e] See text.

2336 | *J. Mater. Chem. A*, 2014, **2**, 2333–2345

This journal is © The Royal Society of Chemistry 2014

3.2 Rh adatoms on ceria(111)

Several possible adsorption sites for the Rh adatom were investigated, including sites above *layer 1a* anions and *layer 1b* cations, all hollow sites (*i.e.* sites above *layer 1c* anions) and bridge sites between any two of them; see Fig. 1b. Two stable structures were found. In the most stable structure, denoted O_H, the Rh is in a three-fold hollow between *layer 1a* anions and above a *layer 1c* anion. At the less stable "bridge" site, denoted O_B, the Rh coordinates to two *layer 1a* anions. In the $p(3 \times 3)$ supercell, there are two inequivalent nearest-neighbour O–O bridge sites, denoted O_{B1}, and O_{B2}. This supercell contains a mirror plane along its long axis (and perpendicular to the plane of the surface itself), as shown in Fig. 1b. Adsorption at O_{B1} maintains this mirror plane, while adsorption at O_{B2} breaks it, so we find slightly different calculated energies for the two sites, although in the large supercell limit they should be equivalent.

In keeping with previous studies, we always find electron transfer from Rh to the surface, with the excess charge localized on a single Ce ion, which becomes nominally Ce^{3+}, and gains a spin of 1 μ_B. This 4f electron can localize on a number of different Ce ions, with the adsorption site (O_H or O_B) interrelated with the localization site. We compare the possibilities in Section 3.2.1 below, before describing the geometric structure and DOS of the most stable one in more detail in 3.2.2. It has been shown elsewhere that there is a hopping barrier for movement of this Ce4f electron through the lattice.[44–46] Hence, in semiconductor terms, Rh adatoms behave as single donors, in the sense of having a single electron that can conduct an electric current in response to an applied electric field.

3.2.1 Rh sites and Ce^{3+} localization patterns. In the $p(3 \times 3)$ supercell there are six possible Ce^{3+} localization sites in the surface triple layer (specifically in T1b), labelled NN_1, NN_2, NNN_1, NNN_2, $NNNN_1$ and $NNNN_2$ in Fig. 2 (other Ce sites are equivalent *via* the PBCs). In the infinite supercell limit, the two NN sites (NN_1 and NN_2) are structurally equivalent, as are the two NNN sites and the two NNNN sites, with identical distances to the Rh. However, in $p(3 \times 3)$ (or any other finite supercell), the shape of the supercell gives the two sites different distances to the nearest periodic images of Rh *via* the PBCs. To see this,
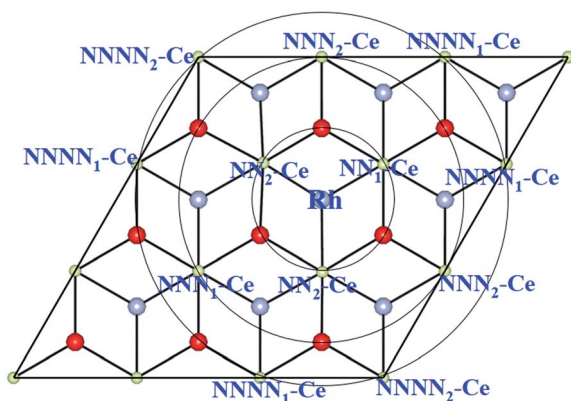
one can extend the shortest line linking the Rh and Ce^{3+} out through the PBCs, back to the Rh. This repeat distance is 20.13 Å for NNN_1, but 10.09 Å for NNN_2. This difference leads, for example, to differences of ∼0.20 eV in the adsorption energies at the two NNN sites.

We find all six charge localization positions to be stable. We also find that these particular localization patterns are intimately linked to the adsorption structure. For *Rh at the O_H site*, we find only localization on NNN sites or further way (attempts to produce, say, O_H-NN_2 relax back to O_{B1}-NN_2). For *Rh at the O_{B1} site*, we find only NN_2 localization, while *Rh adsorbed at the O_{B2} site* can occur with either NN_1 or NN_2 localization (again, attempts to produce O_{B1}-NNN_2, for example, always relax back to O_H-NNN_2). This appears to be a steric effect due, at least in part, to the larger ionic radius of Ce^{3+} as compared to Ce^{4+}. Altogether this gives seven different stable combinations of the
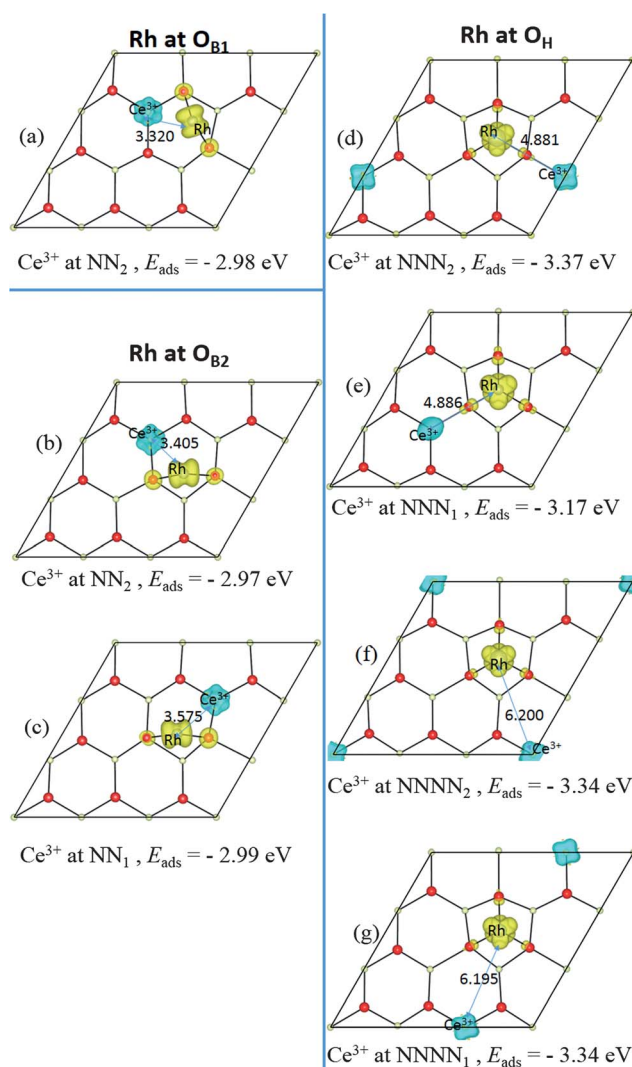

Fig. 3 Top views of the relaxed geometric structures and the spin density ($\rho_{spin\ up}-\rho_{spin\ down}$) for a Rh adatom at the O_{B1} site in (a), O_{B2} site in (b) and (c), O_H site in (d)–(g). In each image, the location of the nominal Ce^{3+} ion from the Ce4f charge localization (at NN_1, NN_2, NNN_2, $NNNN_1$ or $NNNN_2$) is indicated below the image, as is the adsorption energy.

Fig. 2 Schematic top view showing Ce ions within NN, NNN and NNNN shells around Rh adsorbed at the O_H site on the ceria (111) surface.

This journal is © The Royal Society of Chemistry 2014

J. Mater. Chem. A, 2014, **2**, 2333–2345 | **2337**

Table 2 Selected data for energies, structures, charge transfer and local spins for Rh adatom adsorption on the stoichiometric ceria(111) surface

Site and structure^a	$E_{ads}^{gas\,b}$ (eV)	$E_{mag}^{\,c}$ (eV)	$d(Rh-Ce^{3+})^d$ (Å)	$q(Rh)^e$ (e)	$\sigma_{Rh}^{\,f}$ (μ_B)	$\Delta q(Ce^{3+})^g$ (e)	$\sigma_{Ce}^{\,h}$ (μ_B)
$p(3 \times 3)$ supercell							
O_{B1}-NN$_2$	−2.98	0.003	3.32	+0.61	1.45	−0.29	−0.97
O_{B2}-NN$_1$	−2.99	0.003	3.58	+0.50	1.45	−0.27	−0.97
O_{B2}-NN$_2$	−2.97	0.005	3.41	+0.50	1.46	−0.28	−0.95
O_H-NNN$_1$	−3.17	0.002	4.87	+0.62	1.64	−0.27	−0.97
O_H-NNN$_2$	−3.37	0.004	4.88	+0.62	1.64	−0.28	−0.98
O_H-NNNN$_1$	−3.34	0.0001	6.20	+0.64	1.64	−0.26	−0.98
O_H-NNNN$_2$	−3.34	0.0004	6.20	+0.62	1.60	−0.28	−1.00
$p(2 \times 2)$ supercell							
O_H-NNN$_1$	−3.62	−0.002^i	4.83	+0.62	1.67	−0.29	−0.99

^{a} Adsorption sites O_{B1}, O_{B2} and O_H are defined in Fig. 1. The alternative locations of the (nominal) Ce^{3+} ion with respect to the Rh atom are labelled NN$_1$, NN$_2$, NNN$_1$ and so on, as defined in Fig. 2. ^{b} E_{ads}^{gas} is the adsorption energy with respect to a gas phase Rh source (negative value means stabilizing). ^{c} E_{mag} is the energy difference between FM and AFM couplings of the Rh and Ce^{3+} spins. Note that since the structures in the two are almost identical, the errors due to plane-wave cut-off, k-point integration, supercell approximation *etc.* are almost identical. Hence cancellation of errors allows the difference in energy to be much better converged than E_{ads}^{gas} itself. ^{d} $d(Rh-Ce^{3+})$ is the distance between the Rh atom and the (nominal) Ce^{3+} ion. ^{e} $q(Rh)$ is the net charge of the Rh adatom from Bader electron density analysis. ^{f} $\sigma(Rh)$ is the net spin magnetic moment of the Rh adatom from Bader electron density analysis. ^{g} $\Delta q(Ce^{3+})$ is the change in the charge of the reduced Ce ion compared to its charge before the Rh adsorption (+2.38 e) from Bader electron density analysis. ^{h} $\sigma(Ce)$ is the net spin magnetic moment of the Ce ion from Bader electron density analysis. ^{i} Note: FM ground state not AFM.

Rh position and the Ce^{3+} localization pattern. The relaxed structures and spin densities ($\rho_{spin\,up}-\rho_{spin\,down}$) are plotted in Fig. 3a–g, and some energy and structural information is given in Table 2. The most stable has $E_{ads}^{gas} = -3.37$ eV, with the 4f charge localized at a NNN$_2$ site, see Fig. 3d. This is in agreement with the results obtained by Song *et al.*[26], and is very similar to the results found recently for Ce^{3+} localization associated with gold adatoms on a ceria(111) surface,[47] and around oxygen vacancies.[27–29] In the latter case, the preference seems to be for one NN Ce^{3+} and one NNN Ce^{3+}. However, *what we show here* is that the previously reported[26] structure (Rh at the O_H site on ceria (111) with NNN$_2$ localization) is only one possibility out of several, with all the energies lying within 0.4 eV of one another (see Table 2). What is more, the energies of the two NNNN localizations (which are almost degenerate) lie between NNN$_1$ and NNN$_2$, and much closer to the lower energy NNN$_2$. This means that, as NNN$_1$ and NNN$_2$ approach each other in the large supercell limit, the NNNN localization may in fact turn out to be the most stable.

In all of the states shown in Fig. 3 for $p(3 \times 3)$, the spin on the Rh and the spin on the Ce are antiferromagnetically (AFM) coupled. However, we have also found ferromagnetically (FM) coupled versions of each one. Apart from the signs, the spin densities of these FM versions (not shown) are almost indistinguishable from the AFM versions, and the energy difference between the FM and AFM versions is very small (0.0001–0.005 eV, see Table 2) and generally decreases with increasing Rh–Ce separation (see footnote c of Table 2 for comments on convergence).

In the smaller $p(2 \times 2)$ *cell* there are only three possible localizations: NNN$_1$ (= NNN$_2$ *via* the PBCs for this supercell), NN$_1$ and NN$_2$. The NNNN site is indistinguishable from the NN$_2$ site *via* the PBCs, and neither NN$_1$ nor NN$_2$ localization appears to be stable. NNN is stable, with an E_{ads}^{gas} value of −3.62 eV, *i.e.* it is energetically over-stabilized relative to $p(3 \times 3)$ by being NNN in three different directions at once (due to the PBCs). We also find that in $p(2 \times 2)$ the Rh and Ce^{3+} are very weakly FM coupled

rather than AFM. The alternative localizations are missing, since $p(2 \times 2)$ is too small to hold them. Moreover, we find four stable adsorption sites (O_H, O_B, O_T and Ce$_T$) in $p(2 \times 2)$ rather than just two (O_H, O_B) in $p(3 \times 3)$. As a result, issues of magnetic coupling, optimal localization, and available adsorption sites for low densities of Rh adatoms cannot be addressed properly in $p(2 \times 2)$. This would affect the predicted thermodynamics, amongst other things.

3.2.2 Rh at O_H with Ce^{3+} at NNN$_2$: ground state geometric structure and DOS. The geometric structure of the most stable adatom configuration, Rh at O_H with NNN Ce^{3+} localization, is shown in Fig. 4a. The nearest neighbours of the Rh atom are all O, hence giving a Rh–O–Ce chain as reported from EXAFS.[11,13] However, the Rh induces significant geometric changes in the surface, increasing the surface Ce–O bond length by 0.26 Å, so the three NN O atoms and the Rh adatom *are pulled out from the substrate*, as also found in the $p(2 \times 2)$ supercell.[18,21] Fig. 4b shows electronic density of states (DOS) data: the total DOS for the CeO$_2$(111) surface with (panel i) and without (panel ii) the Rh adatom, and projected local DOSs (PDOS) for the adsorbed Rh (panel iii), the closest O (panel iv) and the Ce^{3+} (panel v) ions on the surface. Compared to the clean ceria (111) surface, we see that the O2p–Ce4f gap is now partially filled (panel i, ii). Projections show that this density corresponds to Rh–O bonding states (panel iii, iv).

A Bader charge analysis[48] of the total charge density, given in Table 3, confirms that the Rh adatom has been partially oxidized, losing about 0.6 electrons to the substrate (as also found in the $p(2 \times 2)$ cell[21]). By far the most significant change in the substrate occurs for the single NNN Ce ion, which receives about 0.3 electrons. This value for a nominal Ce$^{4+} \rightarrow$ Ce^{3+} reduction may seem small, but it is very close to that seen in similar calculations for Ce$^{4+} \rightarrow$ Ce^{3+} reductions associated with vacancy creation.[5,36–40] In those studies the change in Ce4f charge (as opposed to the total charge) is around 0.9 electrons,[40]
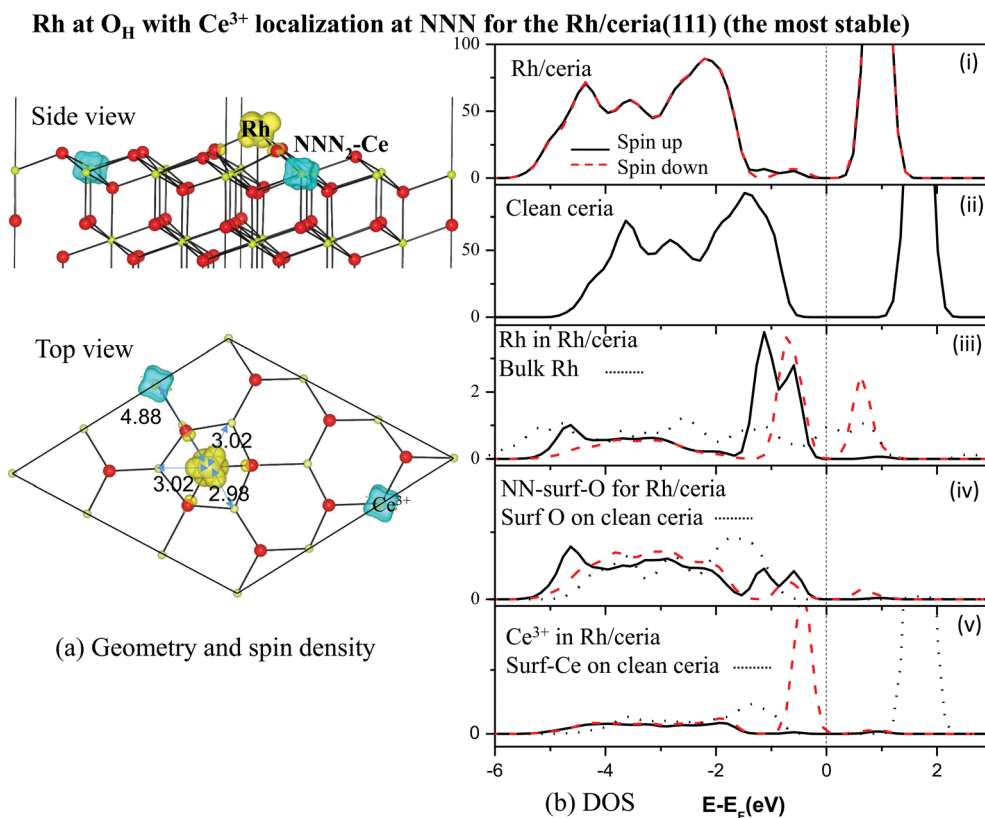
2338 | *J. Mater. Chem. A*, 2014, **2**, 2333–2345

This journal is © The Royal Society of Chemistry 2014

Fig. 4 Rh adatom adsorbed at the O_H site with Ce^{3+} at NNN_2: (a) geometric structures and spin density ($\rho_{\text{spin up}} - \rho_{\text{spin down}}$), and (b) density of states (DOS) in panels (i) and (ii), and Partial DOS (PDOS) in panels (iii)–(v). The vertical dashed line represents the Fermi energy. Thicker black solid and dashed red curves are for spin up and spin down, respectively. The DOS of all other O_H cases are very similar regardless of Ce^{3+} location.

but is partially compensated by an outward redistribution of non-Ce4f charge. In the current case, the degree of transfer assessed by magnetisation is really very complete, with a spin of 0.98 μ_B appearing on the Ce^{3+} ion (Table 3).

Evidently, the Rh adatom is mainly oxidized through charge transfer to the NNN_2 Ce ion, as previously reported,[21,26] but with significant contributions from other nearby ions. Hence at low coverage, we agree with the experimental picture of Ce^{3+} creation via charge transfer[11–13] from Rh to Ce, rather than the picture of a neutral adsorbed Rh only indirectly causing the presence of Ce^{3+} via induced oxygen vacancy formation.[10] We note that the latter picture was based upon the values of the bulk work function of Rh, which will likely be very different from that for mono- or nano-dispersed Rh. The situation can be expected to change when the coverage is sufficient to allow, say, metallic Rh islands or nanoclusters to form.

To summarize: the Rh adatom prefers to adsorb above a subsurface O (O_H site), pulling its three surface layer O neighbours outwards, and transferring charge primarily to a NNN Ce ion on the surface. There are many competing locations for this Ce^{3+} ion, all very close in energy.

3.3   Rh doped ceria surface: Ce site substitution

The geometric structure of a Rh dopant on the Ce sublattice is shown in Fig. 5a. When a nominal Ce^{4+} ion in the T1b layer is replaced by the smaller Rh, the nearest O ions move towards the Rh, with Rh–O bonds of ~2.13 Å. This is smaller than the Ce–O bonds they replace (2.37 Å), but larger than the Rh–O bonds in RhO_2[49,50] and Rh_2O_3[51,52] (~1.97 Å and ~1.80 Å). The strain in the resulting Rh–O and neighbouring O–Ce bonds thus destabilizes the local surface structure, potentially aiding catalytic activity. Similar results have been seen for Au doped ceria.[14]

In its two common bulk oxides, Rh_2O_3 and RhO_2, Rh has (nominal) oxidation states of +III and +IV, respectively, so, from a semiconductor doping point of view, one would therefore naïvely expect Rh when replacing the nominally +IV Ce ion to behave as either (i) an isoelectronic substitution, possibly introducing local distortions to band edges but not to acceptor or donor levels, or (ii) a single acceptor, perhaps able to act as a p-type dopant.

The results of a Bader analysis[48] of our calculated total charge distribution are listed in Table 3, and show no significant extra Ce4f charge or spin density on any Ce ion. The Rh dopant has lost 1.5 electrons and is therefore in a higher oxidation state now as a dopant than when it was as an adatom, but in a lower oxidation state than the Ce it replaced, which had a charge of +2.4 e on the clean $CeO_2(111)$ surface. Since the difference in charge here is 0.9 e, the oxidation state of Rh may be considered to be +III. As a result, the Bader charge of the three NN oxygen ions is only about −1.0 e for each (Table 3), rather than the −1.2 e on the clean surface. These charge

Table 3 Atomic charges (the arrow indicates a range) and spins for the optimized Rh–CeO$_2$(111) systems, from Bader analyses of the most stable Rh adatom case (Rh@O$_H$ and Ce^{3+} at NNN$_2$) and of the most stable Rh-doping case (Rh@Ce-site, no Ce^{3+})

Atomic layers[a]	Groups of atoms in each layer[b]	Rh adatom at the O$_H$ site (with one NNN Ce^{3+}), cf. Fig. 4			Rh substitution on a Ce site in layer T1b, (with no Ce^{3+}), cf. Fig. 5		
		#[c]	Δq^d (e)	Spin^e (μ_B)	#[c]	Δq^d (e)	Spin^e (μ_B)
Rh adatom	Rh adatom	1	+0.62	+1.64			
O in T1a	NNs	3	−0.00 ⇒ +0.07	−0.00 ⇒ +0.01	3	+0.16 ⇒ +0.17	+0.04 ⇒ +0.06
	Others	6	−0.01 ⇒ +0.00	+0.00 ⇒ +0.12	6	−0.01 ⇒ +0.01	−0.00 ⇒ +0.00
Rh dopant in T1b	Rh dopant				1	+1.54	+0.72
Ce in T1b	Ce III	1	−0.28	−0.98	0	N/A	N/A
	Ce IV NNs	3	−0.09 ⇒ −0.01	−0.02 ⇒ −0.00	6	−0.01 ⇒ +0.00	+0.00 ⇒ +0.00
	Other Ce	5	−0.03 ⇒ −0.00	+0.00 ⇒ +0.02	2	−0.05, +0.01	−0.00, +0.00
O in T1c	NNs	0	N/A	N/A	3	+0.08 ⇒ +0.10	−0.01 ⇒ −0.00
	Others	9	−0.07 ⇒ +0.02	−0.00 ⇒ +0.00	6	−0.02 ⇒ −0.01	+0.00 ⇒ +0.00
O in T2a	NN	0	N/A	N/A	1	+0.10	+0.13
	Others	9	−0.02 ⇒ +0.02	−0.00 ⇒ +0.00	8	−0.01 ⇒ +0.03	−0.00 ⇒ +0.00
Σ Over all the above		37	−0.15	+1.01	36	+2.25	+0.98
Σ All other layers		72	+0.15	−0.01	72	+0.14	+0.02
The removed Ce						−2.38 (Ce$^{+2.38}$ ⇒ Ce^0)	

^{a} Data given for the uppermost four atomic layers of ceria and for Rh (as an adatom or as a dopant) in the slab (as shown in Fig. 1), plus the sum over these four ceria layers and the Rh, the sum of the remaining 8 layers. ^{b} The different categories of near neighbours (NNs) refer to the closest O and Ce shells surrounding the Rh, and are listed separately for each layer. ^{c} Columns labelled "#" give the total number of atoms in each group. ^{d} The net charge redistribution (per atom of the type in question) induced by the Rh adsorption, compared to the atomic charges in the stoichiometric ceria(111) slab and a lone Rh atom, obtained from Bader analysis. Hence reference values used: Rh(0.00 e), O(−1.19 e) for layer T1a, and Ce(+2.38 e) for layer T1b, O(−1.16 e) for layer T1c and O(−1.20 e) for layer T2a. ^{e} Atomic spins, obtained from the Bader analysis. Note: a free Rh(g) atom has a spin of 2.18 μ_B.
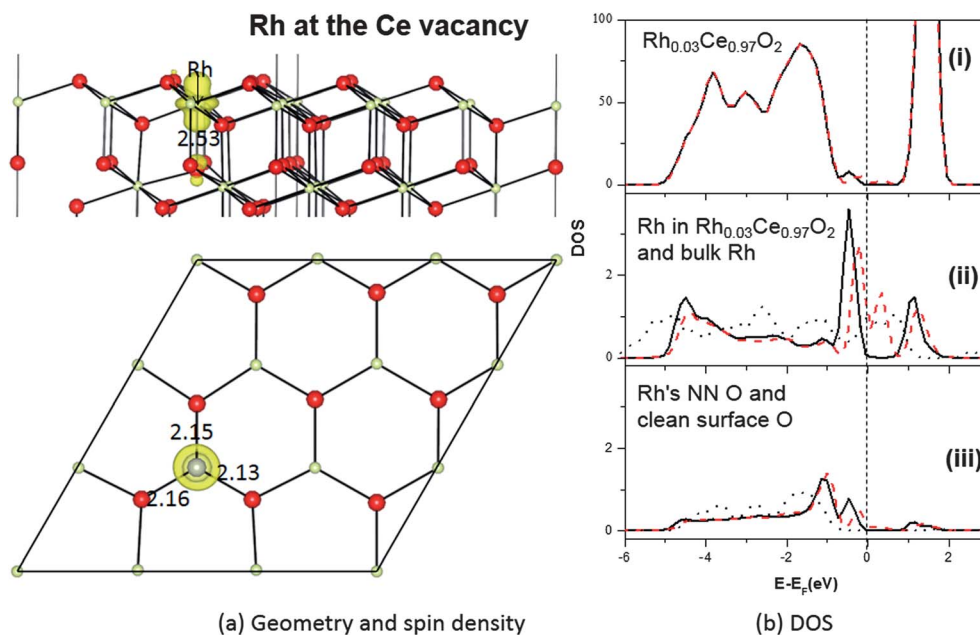
Fig. 5 Rh-doped CeO$_2$(111) system with Rh on a Ce site in the T1b layer: (a) top and side views of the geometric structures and spin density ($\rho_{\text{spin up}} - \rho_{\text{spin down}}$), and (b) DOS curves for (i) total DOS, (ii) bulk Rh (the dotted thin curve) and PDOS for the Rh dopant (the thicker black solid and dashed red curves for spin up and spin down, respectively, here and in other panels), (iii) PDOS of the Rh's NN O and for the corresponding O in the clean ceria(111) surface (the dashed thin curve).

transfers and oxidation assignments are also reflected in the total spin of the doped system, which is about 1.0 μ_B, mainly localized on the 4d states of the Rh dopant (0.7 μ_B) and its neighbouring oxygen ions (Table 3). Hence Rh is behaving roughly as a single acceptor.

The acceptor state itself can be seen in the DOS (Fig. 5b), where a single empty spin down state lies above the Fermi level. However, rather than lying just above the valence band edge it is rather high in the O2p–Ce4f band gap, with filled states in the lower half of the gap. Indeed, there are now DOS features

2340 | J. Mater. Chem. A, 2014, **2**, 2333–2345

This journal is © The Royal Society of Chemistry 2014

Table 4 Projections of the partial charge densities corresponding to the DOS peaks of the occupied and unoccupied states, respectively, within the O2p–Ce4f gap for Rh-on-Ce-site doping of CeO$_2$(111)

Atomic layers[a]	Groups of atoms in each layer[a]	Number of the ions in the group[a]	$n_{electron}$ in filled gap states[b]	$n_{electron}$ in empty gap states[b]
Rh	Rh	1	2.47	0.62
O in T1a	NNs	3	0.55 ⇒ 0.60	0.04 ⇒ 0.06
	Others	6	0.01 ⇒ 0.02	0.00 ⇒ 0.00
Ce in T1b	Ce III	0	N/A	N/A
	Ce IV NNs	6	0.04 ⇒ 0.05	0.01 ⇒ 0.01
	Others	2	0.00, 0.01	0.00, 0.00
O in T1c	NNs	3	0.04 ⇒ 0.04	0.01 ⇒ 0.01
	Others	6	0.01 ⇒ 0.02	0.00 ⇒ 0.00
	NNs	1	0.15	0.11
O in T2a	Others	8	0.00 ⇒ 0.00	0.00 ⇒ 0.00
Σ Over all the above		37	4.92	0.95
Σ Rest of slab		72	0.08	0.05

[a] Atomic layers and groups of neighbours are the same as those used in Table 3. [b] Charges obtained from Bader analyses of the partial charge densities. The arrow indicates a range.

covering almost the entire O2p–Ce4f gap. A Bader analysis (see Table 4) of the partial charge for the filled states (energy window −0.7 eV to 0.0 eV) shows that they are mostly shared between the Rh dopant (2.47 electrons) and its three NN surface O ions (1.71 electrons together), with very little elsewhere (this is similar to what was found in the bulk,[15] except that in the bulk the gap states covered a narrower energy window). Bader analysis of the empty gap states above the Fermi level (energy window 0.0 to 0.7 eV) shows space for exactly one electron, projected mostly on the Rh itself (0.62 electrons) and the four nearest neighbour O ions (0.27 electrons together) (see Table 4). The O and Rh PDOS for the gap states contain similar features, indicating Rh–O bond reorganization, and indeed the gap states resemble filled bonding and partially filled antibonding levels, with strong interactions between Rh4d and O2p.

Putting the Bader and DOS analyses together, it can be inferred that the filled states in the lower part of the band gap would allow Rh on the CeO$_2$(111) surface to act as a deep multiple donor, while the empty state in the mid-gap would allow it to behave as a single deep acceptor. Though useless as a

semiconductor dopant, the presence of this empty DOS state lowers the formation energy for oxygen vacancies, by accepting an extra electron at an energy level below that of the Ce4f state. We will show in Section 3.3 that this does indeed lower the formation energy of vacancies neighbouring Rh dopants in the Ce sublattice.

In the case of Rh doping on the Ce site, there is very little difference at all between the results in $p(2 \times 2)$ and $p(3 \times 3)$, with very similar geometric and electronic structures. The doping energies are also similar, both being very large in comparison with, say, thermal energies under either experimental or growth conditions: $E_{doping} = +5.79$ eV in $p(2 \times 2)$ and +5.44 eV in $p(3 \times 3)$, using gas reference energy for Rh and solid for Ce (the lowest energy combination).

### 3.4 Oxygen vacancy formation in the vicinity of Rh

Rh substitution of a surface O ion, (possibilities 3 and 5 in the list at the start of Section 3.1), may seem like an esoteric construction, but can be viewed as one possible result of Rh adsorption on a partially reduced ceria surface. However, attempts to place a Rh atom on the O sublattice do not succeed for CeO$_2$(111). Instead, the Rh leaves the O site, and moves to the nearest neighbouring O$_B$ adatom site, distorted by the presence of the oxygen vacancy left behind. The structure and spin density are shown in Fig. 6. We here find three nominal Ce^{3+} ions, rather than one. This five-component complex (one vacancy, one adatom and three Ce^{3+} ions) barely fits inside this $p(3 \times 3)$ supercell, so that defect–image interactions *etc.* lead to a rather untidy looking structure. This also leaves little scope for a realistic comparison of different potential configurations of the Rh and Ce^{3+} ions like that reported in Section 3.2.

The E_{doping} value we obtain (−0.54 eV with respect to a gas phase Rh atom source) is meaningless, since the doped structure relaxes back into a vacancy and an adatom (see Fig. 6). However we can extract some useful information from our calculation in two different ways:

We can evaluate the adsorption energy for Rh next to an oxygen vacancy in a (3×3) cell:

$$E_{ads} \text{ next to } V_O = [E(\text{Rh/CeO}_{2-x})] - [E(\text{CeO}_{2-x}) + E_{ref}(\text{Rh})] \quad (5)$$

where $E(\text{Rh/CeO}_{2-x})$ is the total energy of the slab with an oxygen vacancy next to an Rh adatom. E_{ads} next to V_O turns out
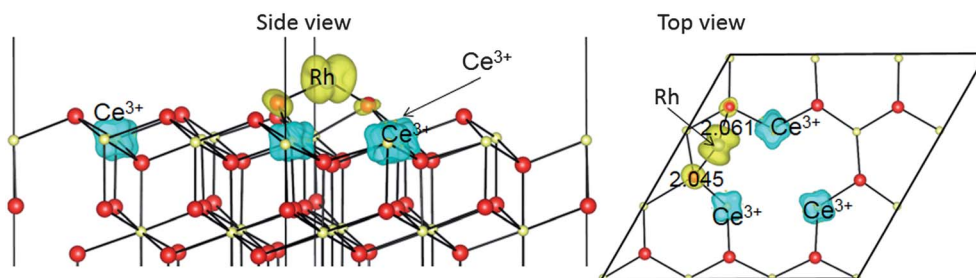
Fig. 6 The geometric structures and spin density ($\rho_{spin\ up} - \rho_{spin\ down}$) for a Rh adatom neighbouring an oxygen vacancy site on CeO$_2$(111), the result of attempting to dope the Rh onto a surface O site on CeO$_2$(111).

This journal is © The Royal Society of Chemistry 2014

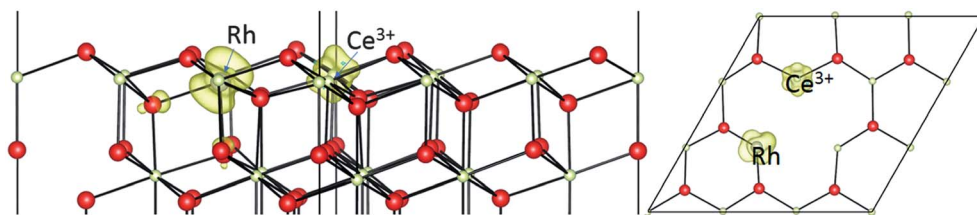*J. Mater. Chem. A*, 2014, **2**, 2333–2345 | **2341**

Fig. 7 The geometric structures and spin density ($\rho_{\text{spin up}} - \rho_{\text{spin down}}$) for an oxygen vacancy neighbouring a Rh ion doped onto a surface Ce site on CeO$_2$(111).

to be −3.20 eV w.r.t. Rh gas, which is 0.17 eV less stable than the values for Rh adsorbed on the stoichiometric surface.

We can also evaluate the formation energy for an oxygen vacancy next to an adsorbed Rh.

$$E_{\text{vac}} \text{ next to Rh-adatom} = [E(\text{Rh}/\text{CeO}_{2-x}) + E_{\text{ref}}(\text{Rh})] - [E(\text{Rh}/\text{CeO}_2)] \quad (6)$$

This turns out to be +2.83 eV. If we calculate the energy for vacancy creation on the clean surface in the same $p(3 \times 3)$ supercell (calculated with the same plane-wave cut-off, k-point grid *etc.*), then we obtain a value of +2.65 eV, which is thus 0.17 eV less than in the vicinity of adsorbed Rh. This corresponds to a slight suppression of V_O formation next to the adsorbed Rh, as calculated in this $p(3 \times 3)$ supercell. In the $p(2 \times 2)$ cell, we find slightly less suppression. This may perhaps imply that in a larger supercell than $p(3 \times 3)$ we would find even more suppression. However, in $p(2 \times 2)$ every single surface ion is part of the vacancy–Rh adatom complex, or is a nearest neighbour to it, with a very distorted position. In other words, there is no undisturbed CeO$_2$(111) surface left within the supercell, so the $p(2 \times 2)$ cell is really too small for these calculations, hence the extrapolation may be unreliable.

We can also consider oxygen vacancy formation next to a Rh ion doped onto the Ce sublattice, as shown in Fig. 7. Vacancy creation in ceria normally involves the transfer of two electrons to localized Ce4f states, leading to two (nominally) Ce^{3+} ions. In this case, we find only one. The second electron has localized on the Rh dopant ion. In other words, it has entered the empty state in the upper part of the O2p $\Rightarrow$ Ce4f gap which we previously found in the PDOS of the Rh dopant, as shown in Fig. 5b.

Since this gap state lies below the Ce4f states, it provides an additional stabilization to the vacancy, so we find that the formation energy for a vacancy nearest neighbouring a Rh doped onto the Ce sublattice is +1.63 eV. This is 1.2 eV lower (less expensive) than in the absence of the Rh. Our 1.63 eV is in reasonable agreement with the value of 1.52 eV reported by Krcha *et al.*[16] using a mirrored slab and a $p(2 \times 2)$ supercell. The reduction in formation energy relative to pure ceria (111) is also similar to the 0.9 eV reduction observed by Aryanpour *et al.*[17] It is interesting to note, however, that we find here a larger increase in activity when the Rh is doped into the surface Ce layer (T1b) rather than the subsurface Ce layer (T2b) as in the calculations of Aryanpour *et al.*

Hence we find a mild suppression of oxygen vacancy creation in the presence of low coverage, atomically dispersed Rh

adatoms on the ceria (111) surface, which would adversely affect the oxygen storage capacity. However, this is countered by a significant enhancement of oxygen vacancy creation (and hence storage capacity) in the presence of single Rh dopants in the surface layer. On the other hand, as discussed in Section 3.3 above, in the absence of cerium vacancies, the formation of Rh dopants on the Ce sublattice is disfavoured at equilibrium, and Rh adatoms should be expected, unless non-equilibrium processes dominate. As a result, the effect of low coverage atomically dispersed Rh on the oxygen storage capacity of ceria (111) is likely to vary, being a complex interplay of the sample history and environment. It should, however, be emphasised that other effects will come into play at larger Rh coverages, especially if the formation of metallic islands and/or nanoclusters is considered.

4. Discussion

4.1 Comparison between the Rh doped and Rh adatom systems

We have found two stable locations for atomically dispersed Rh on the ceria(111) surface: doped Ce$_{1-x}$Rh$_x$O$_2$(111), and Rh adatom/CeO$_2$(111) (the latter with numerous low energy configuration variations). The key differences between the two may be understood as follows: in the Rh adatom–ceria(111) system, the Rh at the centre of the three O anions is mainly oxidized by a Ce^{4+} → Ce^{3+} reduction process on a NNN Ce ion. Meanwhile in the doped Ce$_{1-x}$Rh$_x$O$_2$ system, the Rh atom is oxidized by its NN O ions, and to a higher oxidation state than in the adatom case, although to a lower oxidation state than that of the Ce ion it replaces.

Comparing the two structures, in both cases (adatom or doped), Rh has only O neighbours, in agreement with Hosokawa *et al.*,[11] rather than the Ce-top site suggested by Pfau *et al.*[10] (note also that Rh adatoms lead to the presence of Ce^{3+} ions, even without the vacancy creation assumed by Pfau *et al.*). When comparing our calculated distances with those coming from EXAFS (Table 5),[13] we must bear in mind that the DFT functional we are using, PBE+U, always under-binds, producing overly long bond lengths, and the under-binding worsens with increasing $U > 0$ eV.[3] We obtained a 1.7% overestimation of the bulk lattice parameter, so our calculated Rh–O and Rh–Ce distances must be rescaled for comparison with the experiment. We thus compare Rh–O distances of 2.13 and 2.11 Å for the adatom and doped systems, respectively, with the EXAFS value

2342 | *J. Mater. Chem. A*, 2014, **2**, 2333–2345

This journal is © The Royal Society of Chemistry 2014

Table 5 Comparison of the various calculated Rh–O and Rh–Ce distances ("Dist.") and Rh coordination numbers ("Rh Coord.") with those from EXAFS experiments.[13]

		Calculations (this work).[a] All Rh–X distances < 4 Å are included						Experimental EXAFS[d] ([13])			
		Rh adatom at the O_H site			Rh doped onto the Ce site			Assuming 1% Rh		Assuming 2% Rh	
		Raw dist.[b]	Scaled dist.[c]	Rh coord.	Raw dist.[b]	Scaled dist.[c]	Rh coord.	Distance	Rh Coord.	Distance	Rh Coord.
Rh–O	T1a	2.166	2.130	3	2.149	2.113	3	2.045 ± 0.003	2.2 ± 0.6	2.060 ± 0.005	2.3 ± 0.4
	T1c	2.883	2.835	1	2.210	2.173	3				
	T2a	N/A	N/A	N/A	2.529	2.487	1				
Rh–Ce	T1b	2.985	2.935	3	3.822	3.758	6	3.163 ± 0.004	5.4 ± 0.7	3.157 ± 0.006	5.1 ± 0.5
	T2b	N/A	N/A	N/A	3.820	3.756	3				
Rh–Rh		N/A			N/A			2.722 ± 0.003	5.7 ± 0.3	2.733 ± 0.003	5.4 ± 0.5

[a] Calculated values are from the $p(3 \times 3)$ supercell. Distances, given in Ångströms, grouped by atomic layers, with labels T1a, T1b *etc.* following Fig. 1. All distances below 4 Å are included. [b] "Raw distances" are those obtained directly in the PBE+U calculations. [c] "Scaled distances" have been reduced to correct for PBE+U's 1.7% overestimation of the lattice parameter. This allows easier comparison with experiments. [d] Two sets of EXAFS distances were presented in ref. 13, both from the same set of experimental data, one through fitting under the assumption of 1% Rh doping of the cerium sublattice, the other under the assumption of 2% Rh doping. The EXAFS results find the first shell of O ions around the Rh, followed by a cation shell which contains neighbouring Rh substitutions as well as Ce.

of 2.05 Å. Neither of the theoretical structures match exactly, but neither is inconsistent. However, the experimental coordination number of 2.2 ± 0.6 is more in keeping with the adatom (3 closest neighbours) than the doped system (3 + 3). The Rh–Ce distances differ more. Taking the under-binding into account, we predict 2.94 Å for the adatom and 3.76 Å for the doped Rh, compared to 3.16 Å from the experiment (the coordination numbers in this case are harder to compare, as the models used to fit the experimental data mixed Ce and Rh). Neither of the comparisons are convincing, so overall, we cannot say whether the EXAFS better supports the adatom model or the Ce site doping model, or perhaps a mixture.

Regarding the energetics, the relative stability of the two sites, and the various possible interactions of lone Rh atoms approaching the ceria(111) surface, we find a wide variation in the environment, conditions and sample history. We find that the Rh will never heal an existing oxygen vacancy, or replace a surface oxygen ion, but instead moves to an adatom position, most likely at more than the nearest neighbour distance from the vacancy. For the lone adatom in a vacancy-free region of the surface, the most stable configuration has $E_{ads} = -3.37$ eV relative to Rh vapour. However, if the opposite environmental extreme is considered (hence adsorption relative to Rh metal) $E_{ads} = +2.53$ eV, so that Rh adatoms are then not stable.

For the doped systems, the energy gained from Rh healing of cerium vacancies is always significant (-10.22 eV up to -4.32 eV), but replacement of an existing surface Ce ion always costs energy, with E_{doping} ranging from +5.44 eV up to +14.35 eV. However, these calculated energies each assume some form of equilibrium, so the fact that Rh doping is believed to have been seen experimentally,[13] may be due to non-equilibrium formation processes (such as Ce deficient growth), and kinetic limitations. Indeed, Gayen *et al.*[13] saw indications of three separate Rh sites in their samples, which were prepared by non-equilibrium methods. So, in summary, we may assume that both Rh adatoms and Rh surface doping do occur, depending upon the conditions and sample history.

4.2 Comparison between the $p(2 \times 2)$ and $p(3 \times 3)$ supercells

In most cases we find little difference in electronic or geometric structures between the $p(2 \times 2)$ and $p(3 \times 3)$ supercells. However, some of the structures we have found simply cannot exist in the smaller supercell, including the second most stable structure overall, namely a Rh adatom with Ce4f charge localization at the NNNN distance from the Rh. This inability to tell different Ce4f charge localization patterns apart is obviously important in many situations. Similarly, we find weak AFM coupling to the spin on the Ce^{3+} ion in the $p(3 \times 3)$ cell, but weak FM coupling in $p(2 \times 2)$. Obviously, if these structures or properties are under examination, the larger $p(3 \times 3)$ cell is needed.

Regarding the energetics, we found significant differences between the two cells in some cases, but small changes in others. The problem is that there is currently no known *a priori* way to tell when the difference will be small, or when the larger cell is needed in order to study isolated defects, apart from simply trying it. Indeed, even $p(3 \times 3)$ is a little small: the energies of the NNN_1 and NNN_2 configurations should be equivalent in a large enough supercell, but differ here by $\sim$0.21 eV, with the two NNNN configurations in between. Indeed, we see indications that in a large enough supercell, NNNN might be more stable.

5. Conclusions

Using plane wave DFT with the PBE+U functional, we have studied the geometric and electronic structures and energetics of lone Rh atoms interacting with stoichiometric and non-stoichiometric ceria(111) surfaces. We find that Rh will readily

heal any cerium vacancies present, leading to Rh doping of the Ce sublattice, but it is much less likely to eject and replace an existing Ce ion. Rh healing of oxygen vacancies, or Rh doping into the oxygen sublattice, is never stable. Rh adatoms form readily under most, though not all conditions. In keeping with previous studies,[21,26] we find that the most stable Rh adatom configuration has the Rh in a three-fold hollow site with only oxygen nearest neighbours (three in the T1a surface layer and one in the T1c subsurface layer), together with one Ce^{3+} ion located at the next nearest neighbour (NNN) distance. However, we have shown here that this is only one of a large number of possible configurations, all very close in energy (within 0.4 eV), suggesting that at experimentally relevant temperatures the adatom structure may appear much more dynamic and variable.

We have found some evidence suggesting that, at low coverage, atomically dispersed Rh adatoms would mildly suppress the oxygen storage capacity, while atomically dispersed Rh dopants in the surface layer, which should be much less common than Rh adatoms, would strongly enhance it. Hence the oxygen storage capacity in low coverage Rh–ceria(111) systems should be strongly dependent on sample preparation, history and conditions. At higher (at least local) coverages, other processes may be expected, such as metallic Rh island growth, or Rh nano-cluster growth.

For the Rh-doped ceria(111) system, it is found that the Rh dopant is oxidized mainly by its O neighbours, while at the adatom site it is oxidized mainly by a NNN Ce ion, which converts Ce^{4+} to Ce^{3+}, as also observed experimentally. Hence charge transfer from Rh to CeO_2 occurs in both cases, but in one the transfer is to O2p states and in the other it is to Ce4f.

We have also compared results from the $p(2 \times 2)$ and $p(3 \times 3)$ supercells, and found that in most cases the results are quite similar, although some structures are too large to fit properly into the $p(2 \times 2)$ supercell, and some, but not all, calculated energies can differ significantly between the two supercells. In these cases larger supercells are essential for the study of lone defects.

Returning to our original set of questions:

(i) First it heals Ce vacancies, and then it forms adatoms. It can not easily eject and replace an existing Ce ion, and will never replace an oxygen ion, or heal an oxygen vacancy.

(ii) Rh adatoms have a mild suppressing effect, but Rh dopants strongly enhance it.

(iii) About 0.5–0.7 e, and yes, there is a multitude!

(iv) The results are generally similar, but only when the structure will fit into $p(3 \times 3)$.

Acknowledgements

References

1 A. Trovarelli, *Catalysis by ceria and related materials*, Imperial College Press, 2002.

2 H. C. Yao and Y. F. Yu Yao, *J. Catal.*, 1984, **86**, 254–265.

3 Z. Yang, T. K. Woo, M. Baudin and K. Hermansson, *J. Chem. Phys.*, 2004, **120**, 7741.

4 M. Nolan, S. Grigoleit, D. C. Sayle, S. C. Parker and G. W. Watson, *Surf. Sci.*, 2005, **576**, 217–229.

5 M. Nolan, S. C. Parker and G. W. Watson, *Surf. Sci.*, 2005, **595**, 223–232.

6 W. Kohn and L. J. Sham, *Phys. Rev.*, 1965, **140**, A1133–A1138.

7 S. Bernal, J. J. Calvino, M. A. Cauqui, J. M. Gatica, C. Larese, J. A. Perez Omil and J. M. Pintado, *Catal. Today*, 1999, **50**, 175–206.

8 I. K. Naik and T. Y. Tien, *J. Phys. Chem. Solids*, 1978, **39**, 311–315.

9 A. Pfau and K. D. Schierbaum, *Surf. Sci.*, 1994, **321**, 71–80.

10 A. Pfau, K. D. Schierbaum and W. Göel, *Surf. Sci.*, 1995, **331–333**, 1479–1485.

11 S. Hosokawa, M. Taniguchi, K. Utani, H. Kanai and S. Imamura, *Appl. Catal., A*, 2005, **289**, 115–120.

12 R. Wang, H. Xu, X. Liu, Q. Ge and W. Li, *Appl. Catal., A*, 2006, **305**, 204–210.

13 A. Gayen, K. R. Priolkar, P. R. Sarode, V. Jayaram, M. S. Hegde, G. N. Subbanna and S. Emura, *Chem. Mater.*, 2004, **16**, 2317–2328.

14 V. Shapovalov and H. Metiu, *J. Catal.*, 2007, **245**, 205–214.

15 Z. Yang, G. Luo, Z. Lu, T. K. Woo and K. Hermansson, *J. Phys.: Condens. Matter*, 2008, **20**, 035210.

16 M. D. Krcha, A. D. Mayernick and M. J. Janik, *J. Catal.*, 2012, **293**, 103–115.

17 M. Aryanpour, A. Khetan and H. Pitsch, *ACS Catal.*, 2013, **3**, 1253–1262.

18 H. L. Chen, S. H. Liu and J. J. Ho, *J. Phys. Chem. B*, 2006, **110**, 14816–14823.

19 H.-L. Chen, W.-T. Peng, J.-J. Ho and H.-M. Hsieh, *Chem. Phys.*, 2008, **348**, 161–168.

20 S. Nokbin, K. Hermansson and J. Limtrakul, *Abstr. Papers Am. Chem. Soc.*, 2006, **231**, INOR 247.

21 Z. Lu and Z. Yang, *J. Phys.: Condens. Matter*, 2010, **22**, 475003.

22 B. Li, O. K. Ezekoye, Q. Zhang, L. Chen, P. Cui, G. Graham and X. Pan, *Phys. Rev. B: Condens. Matter Mater. Phys.*, 2010, **82**, 125422.

23 W. Song, A. P. J. Jansen and E. J. M. Hensen, *Faraday Discuss.*, 2013, **162**, 281–292.

24 D. Gerçeker and I. Önal, *Appl. Surf. Sci.*, 2013, **285P**, 927–936, in press.

2344 | *J. Mater. Chem. A*, 2014, **2**, 2333–2345

This journal is © The Royal Society of Chemistry 2014

25 J. Paier, C. Penschke and J. Sauer, *Chem. Rev.*, 2013, **113**, 3949–3985.

26 W. Song, C. Popa, A. P. J. Jansen and E. J. M. Hensen, *J. Phys. Chem. C*, 2012, **116**, 22904–22915.

27 M. V. Ganduglia-Pirovano, J. L. F. Da Silva and J. Sauer, *Phys. Rev. Lett.*, 2009, **102**, 026101.

28 J. Kullgren, K. Hermansson and C. Castleton, *J. Chem. Phys.*, 2012, **137**, 044705.

29 H.-Y. Li, H.-F. Wang, X.-Q. Gong, Y.-L. Guo, Y. Guo, G. Lu and P. Hu, *Phys. Rev. B: Condens. Matter Mater. Phys.*, 2009, **79**, 193401.

30 G. E. Murgida and M. V. Ganduglia-Pirovano, *Phys. Rev. Lett.*, 2013, **110**, 246101.

31 G. Kresse and J. Furthmüller, *Phys. Rev. B: Condens. Matter Mater. Phys.*, 1996, **54**, 11169–11186.

32 G. Kresse and J. Hafner, *Phys. Rev. B: Condens. Matter Mater. Phys.*, 1993, **47**, 558–561.

33 P. E. Blöchl, *Phys. Rev. B: Condens. Matter Mater. Phys.*, 1994, **50**, 17953–17979.

34 S. L. Dudarev, G. A. Botton, S. Y. Savrasov, C. J. Humphreys and A. P. Sutton, *Phys. Rev. B: Condens. Matter Mater. Phys.*, 1998, **57**, 1505–1509.

35 J. P. Perdew, J. A. Chevary, S. H. Vosko, K. A. Jackson, M. R. Pederson, D. J. Singh and C. Fiolhais, *Phys. Rev. B: Condens. Matter Mater. Phys.*, 1992, **46**, 6671–6687.

36 J. L. F. Da Silva, M. V. Ganduglia-Pirovano, J. Sauer, V. Bayer and G. Kresse, *Phys. Rev. B: Condens. Matter Mater. Phys.*, 2007, **75**, 045121.

37 D. A. Andersson, S. I. Simak, B. Johansson, I. A. Abrikosov and N. V. Skorodumova, *Phys. Rev. B: Condens. Matter Mater. Phys.*, 2007, **75**, 035109.

38 L. Christoph, C. Javier, M. N. Konstantin and I. Francesc, *Phys. Rev. B: Condens. Matter Mater. Phys.*, 2007, **75**, 035115.

39 S. Fabris, S. de Gironcoli, S. Baroni, G. Vicario and G. Balducci, *Phys. Rev. B: Condens. Matter Mater. Phys.*, 2005, **71**, 041102(R).

40 C. W. M. Castleton, J. Kullgren and K. Hermansson, *J. Chem. Phys.*, 2007, **127**, 244704.

41 S. Rossignol, F. Gerard, D. Mesnard, C. Kappenstein and D. Duprez, *J. Mater. Chem.*, 2003, **13**, 3017–3020.

42 H. J. Monkhorst and J. D. Pack, *Phys. Rev. B: Condens. Matter Mater. Phys.*, 1976, **13**, 5188–5192.

43 M. Methfessel and A. T. Paxton, *Phys. Rev. B: Condens. Matter Mater. Phys.*, 1989, **40**, 3616–3621.

44 H. L. Tuller and A. S. Nowick, *J. Phys. Chem. Solids*, 1977, **38**, 859–867.

45 C. Castleton, A. Green, J. Kullgren and K. Hermansson, 2014, in preparation.

46 T. Zacherle, A. Schriever, R. A. De Souza and M. Martin, *Phys. Rev. B: Condens. Matter Mater. Phys.*, 2013, **87**, 134104.

47 N. C. Hernandez, R. Grau-Crespo, N. H. de Leeuw and J. F. Sanz, *Phys. Chem. Chem. Phys.*, 2009, **11**, 5246–5252.

48 G. Henkelman, A. Arnaldsson and H. Jonsson, *Comput. Mater. Sci.*, 2006, **36**, 354–360.

49 M. E. Grillo, *Comput. Mater. Sci.*, 2005, **33**, 83–91.

50 G. Demazeau, A. Baranov, R. Pottgen, L. Kienle, M. H. Moller, R.-D. Hoffmann and M. Valldor, *Z. Naturforsch., A: Phys. Sci.*, 2006, **61B**, 1500.

51 A. Wold, R. J. Arnott and W. J. Croft, *Inorg. Chem.*, 1963, **2**, 972–974.

52 Y. D. Scherson, S. J. Aboud, J. Wilcox and B. J. Cantwell, *J. Phys. Chem. C*, 2011, **115**, 11036–11044.

This journal is © The Royal Society of Chemistry 2014

J. Mater. Chem. A, 2014, **2**, 2333–2345 | 2345